JOURNAL OF GEOPHYSICAL RESEARCH, VOL. ???, XXXX, DOI:10.1029/,

Age Characteristics in a Multidecadal Arctic Sea Ice Simulation

Elizabeth C. Hunke

T-3 Fluid Dynamics and Solid Mechanics Group, Theoretical Division, Los Alamos National Laboratory, Los Alamos, New Mexico, USA

Cecilia M. Bitz

Atmospheric Sciences, University of Washington, Seattle, Washington, USA

E. C. Hunke, MS-B216 Los Alamos National Laboratory, Los Alamos, NM 87545, USA. (eclare@lanl.gov)

C. M. Bitz, Atmospheric Sciences box 351640, University of Washington, Seattle WA 98195-1640 USA. (bitz@atmos.washington.edu)

Abstract. Results from adding a tracer for age of sea ice to a sophisticated sea ice model that is widely used for climate studies are presented. The consistent simulation of ice age, dynamics, and thermodynamics in the model shows explicitly that the loss of Arctic perennial ice has accelerated in the past three decades, as has been seen in satellite-derived observations. Our model shows that the September ice age average across the Northern Hemisphere varies from about five to eight years and the ice is much younger (about two to three years) in late winter due to the expansion of first-year ice. We find seasonal ice on average comprises about 5% of the total ice area in September, but as much as $1.36 \text{x} 10^6$ km^2 survives in some years. Our simulated ice age in the late 1980s and early 1990s declined markedly in agreement with other studies. However, after this period of decline, the ice age began to recover. As a result we find little trend in the average ice age over the last two decades. In contrast, ice area, thickness and volume declined over the same period, particularly for perennial ice, with an apparent acceleration in the last decade.

1. Introduction

The sea ice cover in the Northern Hemisphere is undergoing significant changes, the most threatening being a shift from a mostly perennial pack to an ice cover dominated by seasonal ice, as in the Antarctic [*Rigor and Wallace*, 2004; *Maslanik et al.*, 2007]. This is of fundamental concern for native peoples and wildlife that depend on the pack ice for their livelihoods. We do not yet know the magnitude of potential future climate change that could be associated with such a shift in the Arctic, but climate models indicate that sea-ice related feedbacks contribute to polar amplification of the global warming signal [e.g., *Holland and Bitz*, 2003].

Beginning in the late 1970s, the satellite era opened a viewing window for the large-scale variability of the polar regions. While the satellite record is limited in length and consists primarily of sea ice area concentration deduced from brightness temperatures [*Gloersen et al.*, 1992], substantive changes to the Arctic sea ice pack over the past decade are becoming apparent nevertheless, particularly as reductions in area coverage in summer [e.g., *Comiso et al.*, 2008]. Although more difficult to observe, other fundamental characteristics of the pack ice are also changing, such as ice thickness [*Wadhams*, 1990; *Rothrock et al.*, 1999; *Wadhams and Davis*, 2000]. Several factors influence whether ice survives the melt season, including thickness [*Untersteiner*, 1961], variations in atmospheric and oceanic temperature and circulation patterns [*Comiso et al.*, 2003], and the duration of the melt season [*Belchansky et al.*, 2004].

Efforts to infer or measure other variables from satellites, such as sea ice thickness and velocity, is progressing [e.g., *Laxon et al.*, 2003; *Kwok et al.*, 2004a], and synthesis of technologies enable derivation of additional quantities. In light of research suggesting recent thinning of Arctic sea ice [e.g., *Rothrock et al.*, 1999], and in the absence of basin-wide, detailed thickness observations, there has been much interest in obtaining ice age estimates from satellite data, with which to infer and understand changes in the volume of Arctic sea ice. Ice thickness is closely related to the age of the ice, because thickening through growth and ridging accumulates over time. *Johannessen et al.* [1999] initiated the effort using satellite passive microwave data for November through March, 1978–1998. Surface emissivities of open water, first-year and multi-year (perennial) ice are sensitive to the sensor frequency and if they are assumed to be relatively stable in winter, ice age can be crudely distinguished. *Johannessen et al.* related trends in perennial ice area to thickness changes inferred from surface elastic-gravity wave measurements.

However, the stability assumptions of their method are questionable [*Comiso*, 2002; *Fowler et al.*, 2004]; *Comiso* [2002] simply defined multi-year ice to be that ice remaining at the end of the summer melt season in September, determined from a 7-day running mean of satellite-derived minimum ice extent for 1978–2000. In a different approach, *Rigor and Wallace* [2004] fed monthly gridded ice motion fields from Arctic buoys [*Rigor et al.*, 2002] and September ice concentration data into to a simple advection model, tracking the ice until the following September. Ice remaining within the 90% ice concentration contour was aged one year. Using this procedure, they obtained ice age estimates for the last several decades, through 2002. *Fowler et al.* [2004] employed a similar technique, but using daily Advanced Very High Resolution Radiometer (AVHRR) ice velocities, averaged to weekly, and a 40% ice concentration threshold. *Belchansky et al.* [2005] also used an ice-tracking approach, but backwards in time, generating ice age maps for 1989–2003 by aging pixels within the 15% concentration contour each month, until reaching the time and location of the ice's origin. *Nghiem et al.* [2007] returned to the ideas of *Johannessen et al.* [1999], exploiting distinctive backscatter signatures from the QuikSCAT satellite to identify seasonal, perennial, and a "mixed" ice class. Finally, *Maslanik et al.* [2007] used the *Fowler et al.* [2004] approach, coupled with ICEsat laser altimeter ice thickness data for 2003–2006, to develop an ice thickness proxy that could be used to create maps of ice volume in prior years via thickness correlations with satellite-based ice age.

The overall results from these various methods are similar, although they differ in the details. All indicate a reduction in area of older ice types in the Arctic over the past several decades, in general agreement with observations of a thinning ice pack. The eastern Arctic Ocean is dominated by younger ice, while older ice resides in the western Arctic, in and near the Canadian Archipelago. Perennial ice classes are recruited from first-year ice formed primarily in the eastern Arctic and north of Alaska. Some of this ice is entrained into the Beaufort Gyre where it recirculates, ridging and thickening until it is ejected into the Transpolar Drift Stream, which carries ice across the North Pole and out of the Arctic through Fram Strait. Northward retreat of the summer ice edge from the North American coast has cut short the recirculation of ice in the Beaufort Gyre, leaving thinner ice that melts more easily in the gyre [*Rigor and Wallace*, 2004; *Belchansky et al.*, 2005; *Maslanik et al.*, 2007].

Older ice, and by association thicker ice, possesses different characteristics than younger, thinner ice by virtue of the aging process, particularly desalination through brine channels and associated changes in albedo [*Perovich*, 2003]. Changes in the physical characteristics of the ice pack due to its transition from older to younger ice will have ramifications for the strength of feedbacks [*Perovich et al.*, 2008] and ecosystem structure [*Lizotte*, 2001].

No studies of sea ice age to date have used a full-physics sea ice model with a consistent method for determining age and thickness. Here we present a 59-year Arctic simulation with a new implementation of the Los Alamos sea ice model, CICE version 4.0, which includes a representation of sea ice age.

2. Model description

The sea ice model employed here, CICE version 4.0, features many software and physics enhancements over previous versions. The model infrastructure was thoroughly overhauled for improved performance and flexibility, including a straight-forward mechanism for adding tracers such as ice age, melt ponds, and biological or chemical compounds that are carried on (or in) the ice and snow. A tracer already found in a few sea ice models (e.g., previous versions of CICE) is surface temperature, which evolves thermodynamically and is transported with the ice as

$$\frac{\partial (a_{in} T_n)}{\partial t} + \nabla \cdot (a_{in} T_n \mathbf{u}) = 0, \tag{1}$$

where a_{in} is the ice area fraction of thickness category n, T_n is the tracer quantity in category n, $\mathbf{u}$ is ice velocity and t represents time. Transport of other tracers may be volume weighted, in which case the transport equation takes the form

$$\frac{\partial (v_{in} T_n)}{\partial t} + \nabla \cdot (v_{in} T_n \mathbf{u}) = 0. \tag{2}$$

Transport of snow volume tracers would use the snow volume, v_{sn}, instead of the ice volume, v_{in}. In CICE, ice age is an ice volume tracer following equation (2).

In CICE, modeled ice and snow volumes fluctuate due to thermodynamic growth and melt following *Bitz and Lipscomb* [1999], horizontal transport via incremental remapping [*Lipscomb and Hunke*, 2004], and mechanical redistribution (that is, rafting and ridging), based on *Thorndike et al.* [1975], *Rothrock* [1975], *Hibler* [1980], *Flato and Hibler* [1995], *Bitz et al.* [2001] and *Lipscomb et al.* [2007]. Ice is transferred among thickness categories using the remapping scheme of *Lipscomb* [2001]. We use the elastic-viscous-plastic (EVP) ice dynamics model of *Hunke and Dukowicz* [2002], as modified by *Connolley et al.* [2004], to find the ice velocity. Velocity components are used for horizontal ice transport, and spatial derivatives of velocity (ice deformation or strain rates) drive the mechanical redistribution.

The incremental remapping scheme is conservative, non-oscillatory, second-order accurate in space, and monotonicity-preserving for tracers; that is, it does not create new extrema. The accuracy may be reduced locally to first order to preserve monotonicity. The characteristic that sets incremental remapping apart from other advection schemes is that it is efficient for large numbers of thickness categories or tracers. Much of the work needed to remap spatial quantities from one time step to the next is geometrical and performed once per grid cell. Additional categories or tracers utilize the existing geometrical information, requiring only a small amount of extra work [*Lipscomb and Hunke*, 2004].

In the configuration used here, CICE partitions the ice pack in each grid cell into a 5-category ice thickness distribution, with 4 ice layers and 1 snow layer in each category. State variables for each thickness category include ice area and surface temperature, plus ice or snow volume and enthalpy for each layer within each thickness category. (The thickness category ranges are 0–0.64 m, 0.64–1.39 m, 1.39–2.47 m, 2.47–4.57 m, and greater than 4.57 m.) Because ice volume is the product of area and thickness, $v_{in} = a_{in}h_{in}$, ice thickness can be considered an ice area tracer (Eq. 1). Similarly, enthalpy is an ice volume tracer. Counting all of these tracers, plus ice age, in all categories and layers, CICE carries 45 tracer fields in addition to ice area. Although all state variables and tracers are defined and modeled for each thickness category, for output and analysis the category values are merged into a single value for each grid cell using the category ice concentrations (or volumes, for volume tracers). Age "classes" or "types" referred to in this paper are defined during the post-processing stage and used to collect ice of similar ages for analysis.

Tracers may or may not affect the physical evolution of the pack. Although physical characteristics of the ice are known to change as the ice ages (salinity reduction via brine drainage, for instance), these changes are directly related to physical conditions, and we therefore treat ice age as a passive tracer. Initialized at age 0 upon freezing in open water (e.g., frazil production), ice ages the length of the time step at each step. Melting does not affect the age. In our control run, basal freezing also does not alter the age, but we present results from a sensitivity run in which basal freezing makes the ice column younger. Mechanical redistribution processes and advection alter the age of ice in any given grid cell in a conservative manner following changes in ice volume.

The model is configured for the global 320 × 384 (1°), displaced-pole grid used for the ocean and ice components of the fully-coupled Community Climate System Model version 3 (CCSM3) [*Kiehl and Gent*, 2004; *Collins et al.*, 2006], using a one-hour time step. The grid spacing ranges between 20 and 85 km, averaging 40 km north of 70 N. Output from the CCSM ocean component (POP) in a fully-coupled CCSM run is used for the lower boundary conditions in CICE, including sea surface temperature, salinity and a deep ocean heat flux. Ocean currents are set to zero. The sea surface temperature is computed using a thermodynamic ocean mixed layer parameterization within CICE, which depends on prescribed atmospheric forcing and the sea ice evolution.

Atmospheric forcing data includes 6-hourly air temperature, specific humidity, and wind velocity components from the Common Ocean Reference Experiments (CORE) version 2 [1958-2006, *Large and Yeager*, 2008] along with monthly "normal year" precipitation from version 1 [*Large and Yeager*, 2004], as described in *Hunke and Holland* [2007]. Rather than reading data for shortwave and longwave radiation, we use version 2 of the Ocean Model Intercomparison Project's cloud climatology [OMIP, *Röske*, 2001] along with temperature and humidity data to compute these fields following the Arctic Ocean Model Intercomparison protocol [*Hunke and Holland*, 2007]. A stability-based atmospheric boundary layer formulation is used to compute the turbulent sensible and latent heat fluxes and wind stress components. The sea ice albedo follows the dual-band, thickness- and temperature-dependent formulation of CCSM3. Further information regarding CICE can be found in *Hunke and Lipscomb* [2008].

The ice state is initialized from an earlier run, as described in *Hunke and Holland* [2007]. Although fast ice in a few grid cells in the Canadian Arctic reaches ages concomitant with the length of the run, which starts in 1958, most of the pack achieves its oldest values by the mid-1970s, and we analyze the last 30 years of output.

3. Results

First, we clarify a point of semantics. In the nomenclature used by the World Meteorological Organization [*WMO*, 1989], *first-year ice* is "sea ice of not more than one winter's growth, developing from young ice; thickness 30 cm–2 m." Thus, young ice less than 30 cm thick is not classified as first-year ice. *Old ice* is "sea ice which has survived at least one summer's melt ... May be divided into *second-year* and *multi-year* ice." Second-year ice has survived only one summer's melt, while multi-year ice has survived at least two summers' melt. At the end of summer, ice which grew late in the preceding winter and is less than one year old is reclassified as second-year ice. This nomenclature is quite sensible for field observations but leads to confusion when comparing with a numerical age tracer such as ours. In the spirit of the WMO nomenclature, *Belchansky et al.* [2005] classify 0–4-month-old ice as "first-year," 5–15-month-old ice as "second-year," and so on. Other studies include second-year ice (as defined by the WMO) in their multi-year ice class [*Johannessen et al.*, 1999; *Comiso*, 2002; *Maslanik et al.*, 2007]. Following the lead of *Nghiem et al.* [2007], we refer to ice which is less than 1 year old as "seasonal" ice and ice older than 1 year as "perennial" ice, otherwise following the WMO nomenclature or that used by the cited authors, in context.

3.1. Seasonal and perennial ice

We begin with an inspection of Northern Hemisphere total ice volume and area coverage, broken down into seasonal and perennial ice types. Of these, the most easily compared with observations is total ice area, shown in Figure 1a. The maximum and minimum values compare well with satellite passive microwave data for 1978–1987 [13.9×10^6 km^2 and 4.7×10^6 km^2, respectively, *Gloersen et al.*, 1992]. The ice edge, especially in winter, is strongly controlled by the amount of heat available from the ocean [*Bitz et al.*, 2005], and because ice area concentration is nearly 100% in winter, the same is true for total winter ice area. Here, ocean heat flux from a CCSM simulation is input as an annually repeating monthly-mean climatology and hence the resulting total ice area simulation varies little from year to year at its winter maximum. Interannual atmospheric variability becomes more prevalent in warmer months when albedo feedbacks intensify and the ice edge retreats from regions with strong ocean heat flux convergence.

In contrast, the area covered by perennial ice fluctuates from year to year even in winter, as indicated in Figure 1b, and represents a significant influence on the total volume of perennial ice. Seasonal ice area in this simulation (Figure 1c) is the difference between the total ice area and the perennial ice area, and hence it also is constrained by the prescribed oceanic heat flux in winter. In summer, seasonal ice occasionally disappears altogether, but up to 1.36×10^6 km^2 survives to become perennial ice in some years (Fig. 1d). By September, on average only 5% of the total ice area is seasonal ice. However, the September total ice area anomaly, also shown in Fig. 1d, is correlated with the September seasonal ice area with a correlation coefficient of 0.54 when linear trends are removed (the correlation is for the period 1977–2006 and is significant at the 95% confidence level).

Although the total volume of seasonal ice is somewhat limited by the length of time during which it can grow, so that it remains relatively thin compared with older ice, it nevertheless contributes significantly to the seasonal cycle of total ice volume; the amplitude of the seasonal cycle of perennial ice volume is about 6×10^3 km^3 (Figure 1b), while the total volume cycle is roughly 13×10^3 km^3 (Figure 1a), the remainder being made up of $\sim 7 \times 10^6$ km^2 of $\sim$ 1-m young ice.

Transport of ice through Fram Strait into the North Atlantic, where it melts, is known to be a significant factor in the loss of Arctic perennial ice types [*Rigor and Wallace*, 2004; *Nghiem et al.*, 2007]. The model simulates this transport well, as compared with satellite-based observational data [*Kwok et al.*, 2004a] (Figure 2), although the variability of fluxes is larger in the simulation than in the observations. The flux gate used for analysis of the satellite data is in a slightly difference place than the grid line used for the model calculation; the endpoints of the flux gate for the model estimates are (79.9N, 16W) and (80.3N, 20E).

Figure 1e shows the Northern-Hemisphere-average sea ice age for perennial and all ice classes. Perennial ice reaches a quasi-equilibrium age by the mid-1970s. The maximum value during each year occurs at the end of summer, when perennial ice area is as its minimum. In the early 1980s the area covered by younger ice shrank, causing the maximum in ice age seen here in 1981. This is associated with the extended period of high ice flux through Fram Strait (Figure 2) and will be discussed in more detail later.

The mean annual cycle of perennial ice volume, area, thickness and age for three decades beginning in 1977 is shown in Figure 3. The simulation indicates that loss of perennial ice volume has accelerated, in agreement with satellite-derived observations [*Comiso*, 2006; *Nghiem et al.*, 2007; *Comiso et al.*, 2008], primarily due to decreasing ice thickness. Interestingly, the average ice age had little trend in the past two decades, following a 1-year shift to younger ice after 1981.

Statistics for the full 1977–2006 period, given in Table 1, highlight the trend of seasonal ice partially replacing perennial ice in March, with a net decrease in area overall and a concomitant reduction in average age. Both ice types are declining in September.

3.2. Sea ice thickness and age

Maslanik et al. [2007] used ice age and ice thickness from March satellite observations during 2003–2006 (as described in the Introduction) to obtain a proxy data set of ice thickness, assuming that older ice is thicker than younger ice. Their results are shown in Figure 4 against the output from our model simulation. Agreement is remarkably good for ice up to 10 years old. Five- to eight-year-old ice was slightly thicker in earlier decades. Ice beyond 10 years of age continues to age but at a hemispherically averaged rate slower than actual time. For instance, by the end of the second decade illustrated here, the simulation has run for 39 years, but there is no ice older than 26 years in the hemispheric average. This discrepancy is due to the incorporation of first-year lead ice within the pack and from the marginal ice zone.

Neither spatial patterns nor interannual variability of ice age and ice thickness are as closely related as might be deduced from the *Maslanik et al.* [2007] proxy. Figure 5 illustrates modeled ice thickness and age in March of 1976, 1986, 1996 and 2006. Near the Canadian Archipelago, where ice is very thick and old, and near the Siberian coast, where ice tends to be thin and young, the age and thickness contours line up well. In the central Arctic, however, dynamic processes contribute to the complexity of the pack's physical characteristics through large-scale ice motion (Beaufort Gyre, transpolar drift and export through Fram Strait) and smaller scale processes such as rafting and ridging.

In our simulation, the oldest ice is consistently located in the Canadian Arctic where the pack is thick and relatively stationary. Looking only at the central Arctic Ocean region (i.e., excluding the Canadian Arctic), we see that the Beaufort Gyre holds the oldest ice in 1976, which continues to age as it recirculates [*Rigor and Wallace*, 2004]. By 1986 a band of older ice reaches across the southern Arctic Ocean from northern Greenland west to eastern Siberia, encircling a bight of younger ice. This pattern reflects both the Beaufort Gyre's circulation pattern and the Transpolar Drift's large export of ice through Fram

Strait a few years earlier. In 1996 older (and thicker) ice is compressed along the Canadian Archipelago, with indications of transport around the southern flank of the Beaufort Gyre. By 2006 the central Arctic has refilled with older ice, although it is neither as old nor as thick as that seen in previous decades.

Interannual variability of ice age does not have a strong positive correlation with ice thickness, volume, or extent when averaged north of 70N or for the whole Northern Hemisphere (see Figure 1). The strongest relation we found was in fact a *negative correlation* between September ice age and September area (r = -0.68, significant at greater than 95% confidence level). The negative correlation derives from the fact that anomalously low seasonal ice coverage leaves a proportionately above-average amount of perennial ice behind, which causes the ice that remains to be older than average while at the same time giving rise to anomalously low ice area.

3.3. Processes affecting sea ice age

Ice volume at any given point in time represents a time-integrated history of the many processes acting on sea ice. Similarly, ice age reflects both calamity and serenity during the unrelenting march of time. Figure 6a illustrates these contrasts in the form of a Hovmüller diagram. The area coverage of one- to six-year-old ice is fairly constant from the mid-1970s through 1990, indicating fairly consistent conversion from younger ice types. The 1981 maximum in ice age seen in Figure 1e is evident here as a moderate reduction in the area of roughly two- to six-year-old ice beginning in 1980, while older ice types maintain their coverage. During the 1990s, however, larger areas of younger ice are present while ice classes older than 6 years fail to be repopulated. The younger ice types gradually age until six-year and older ice is replenished in the mid-2000s. Meanwhile during the last decade of the run, area coverage by the youngest ice types diminishes, leading to the relatively old maxima in average ice age seen at the end of the run (Figure 1e).

Figure 6b illustrates these changes in a slightly different way, as the cumulative area of ice older than a given age. The cumulative presentation emphasizes the transient features, making it easier to see a temporary reduction in two- to six-year-old ice in the early 1980s. The mid-1990s show a unique reduction in six-year and older ice after the prolonged loss of younger ice that would normally replenish the older ice classes. As a result, the basin-wide average age reaches a minimum in 1997. Our results agree with *Belchansky et al.* [2005], who observed that considerable areas of first-year ice survived the melt season in the mid-1990s (see spikes in the 1992 and 1996 in our Figure 1d), which then rebuild multi-year ice area in the late 1990s. However our results also show that the repopulation of multi-year ice classes was only temporary: younger ice types again declined in the 2000s.

Our results also broadly agree with those of *Rigor and Wallace* [2004], who use an advection model with observational input data. However, our ice tends to be younger than theirs in the 1980s because deformation in our model ridges and rafts younger, thinner ice, effectively lowering the age of older, thicker ice. By the end of summer in the 1980s, most of the Arctic in *Rigor and Wallace*'s study was covered by ice older than 10 years; in contrast our Northern-Hemisphere-average ice is generally about 7 years old at the end of summer in the 1980s (Fig. 1e). By September 2002, most of the ice age in *Rigor and Wallace*'s study is less than 5 years old; at the same time our model ice age still averages between 6 and 7 years. Furthermore, our model clearly indicates that the declining trend in ice area and thickness is not commensurate with a consistent loss of ice of any particular age, nor a decline in average ice age overall.

We find it more difficult to compare with the studies of *Maslanik et al.* [2007] and *Fowler et al.* [2004] because their figures combine all ice greater than 5 years of age in one bin. They discuss ice age differences between years with apparent extrema, rather than trends; the range of our extrema are similar to theirs. Their ice age appears to show some recovery in the early 2000s, as does ours and that of *Belchansky et al.* [2005].

Dynamical processes act to decrease the volume of older ice in two ways: first by incorporating younger ice into the old through advection and mechanical deformation, and second by transporting ice to the marginal ice zone where it melts. In our simulation, the transport of ice through Fram Strait (Figure 2) is a strong dynamical influence on the age characteristics of the Arctic sea ice pack. Two- to six-year-old ice comprises much of the Fram Strait ice export, which all melts eventually. The extended period of high flux rates in the early 1980s carried much young ice out of the Arctic (Figure 6c), depleting these age classes and resulting in the flux of 6-year and older ice through Fram Strait in subsequent years. 1986 saw another period of young ice export, but rates were low (Figure 2). In the late 1980s flux rates again increased, this time carrying much older ice. This resulted in the depletion of older ice types seen in the early 1990s [*Rigor and Wallace*, 2004].

Kwok and Rothrock [1999] and *Rigor et al.* [2002] examine the correlation of ice fluxes through Fram Strait with the North Atlantic and Arctic Oscillation (AO) indices. Briefly, high AO signals in winter are associated with increased advection of ice away from the Eurasian coast and through Fram Strait, while low AO conditions lead to more open water in the Beaufort and Chukchi Seas and increased circulation of the Beaufort Gyre, which carries more ice to the marginal ice zone north of Alaska [*Rigor and Wallace*, 2004]. The AO was substantially higher than normal from late 1988 through 1994 and more neutral since 1995, except for a moderately high period in 2000–2002 and again in 2007. Our simulation suggests that the ice age began to recover in 1996, despite the fact that the declining trend in ice area and thickness continued. These results suggest that the AO has a large influence on ice age, but the decline in actual area and thickness is more a function of the increase in greenhouse warming. This suggestion is supported by the fact that in 20th and 21st century projections by global climate models, ice area and thickness tend to decline considerably [e.g., *Arzel et al.*, 2006; *Zhang and Walsh*, 2006] with little or no trend in the AO [*Gillett et al.*, 2002].

A typical indicator of basin-wide thermodynamic effects is melt season length, or dates of melt or freeze onset. Using satellite passive microwave measurements of brightness temperature in conjunction with National Center for Environmental Prediction (NCEP) reanalysis surface air temperatures for 1979–1996, *Smith* [1998] found an increase in melt season length of 4.5 days per decade for perennial ice within the Arctic Ocean. Using an updated algorithm, *Belchansky et al.* [2004] estimated the analogous change in melt season length at 5.5 days per decade. We compute a similar positive trend of 6.7 days per decade for the full Northern Hemisphere (Table 2). Differences in melt season length stem from differences in the analyzed area (Arctic Ocean versus Northern Hemisphere) and algorithms for identifying perennial ice as well as the method for identifying melt and freeze onset dates. Seasonal ice was not experiencing as drastic a change as perennial ice; our modeled trend in melt duration for all Northern Hemisphere ice is an increase of 4.7

days per decade for 1979–1996. For the 1979–2006 period, however, the melt duration for seasonal and perennial ice types both increased 6.5 days per decade.

3.4. Ice column age

In the simulation described above, the addition of new ice on the bottom of existing ice did not affect the age of the ice in that thickness category, so that our results would be more comparable to those derived from satellite observations. To find out how sensitive the sea ice age is to vertical thermodynamic accretion, we performed a second simulation identical to the first except that the volume of new bottom ice is given an initial age equal to the time step ($\Delta t = 1$ hr) which is then volume-averaged with the age of the existing ice. Spatial patterns in the resulting age maps are similar to the control run results, but the ice is much younger overall, as is evident in Figure 7, highlighting the prominent role that seasonal ice already plays in the Arctic. Not only is it a significant—and growing—fraction of the total area covered by sea ice on a seasonal basis, new ice at the bottom of the ice column reduces the average “true” age of the pack and contributes its own physical properties to the ice column.

Some of the ice accreted onto the bottom of the pack melts, resulting in a loss of relatively young ice from the ice column. In this simulation we do not track the age of ice layers within the ice column, only the average age of the ice thickness category, and are thus unable to adjust the age appropriately upon melting. Therefore this sensitivity test represents a lower bound for the age of the ice pack.

4. Conclusions

Sparsity of high latitude, *in situ* observational data has led researchers to clever uses of satellite and ground-based measurements. Total ice volume remains just out of reach, although thickness estimates are becoming available [e.g., *Kwok et al.*, 2004b]. As remote sensing technology progresses, combinations of techniques may enable us to reconstruct the history of the polar ice cover, as *Maslanik et al.* [2007] demonstrate with their ice thickness proxy. In the meantime, sea ice models such as CICE attempt to fill in the gaps, particularly subsurface processes that satellites can not see.

In CICE, each thickness category in the ice-thickness distribution has a unique thickness, ice age, concentration, snow depth, temperature profile, albedo, and set of surface fluxes. Ice motion is computed by the model with a one-hour time step for the velocity field, ice advection, and deformation. The model is forced with six-hourly varying atmospheric conditions for 1958–2006. Thus our model computes ice age in a consistent fashion with evolution of ice dynamics and thermodynamics. In contrast, previous studies that presented ice age in detail used observations to derive ice motion, deformation, and extent, with an advection and deformation time step of one month [*Rigor and Wallace*, 2004] or one week [*Fowler et al.*, 2004; *Maslanik et al.*, 2007]. *Rigor and Wallace* [2004] use an empirical relation to estimate ice growth that is independent of snow depth and atmospheric conditions. *Fowler et al.* [2004] and *Maslanik et al.* [2007] do not model ice growth or melt processes, instead using satellite imagery to determine areas of ice loss or new ice growth.

The consistent simulation of ice age, dynamics, and thermodynamics in our model agrees well with the large spatial-scale, multi-year, average sea ice thickness–age relation that was derived from observations by *Maslanik et al.* [2007]. Our model shows explicitly the accelerating loss of perennial ice over the past three decades that has been seen in satellite-derived observations [*Nghiem et al.*, 2007; *Comiso et al.*, 2008].

Our model also shows that the September average ice age across the Northern Hemisphere varies from about five to eight years and the ice pack is much younger (about two to three years) in late winter due to the expansion of first-year ice. We find first-year ice on average comprises about 5% of the total ice area in September, but as much as 1.36 x10^6 km^2 survive in some years. Seasonal ice area in September has not declined significantly in recent decades, thus the declining trend in total area in September is a result of the decline in perennial ice area. Nonetheless, interannual variability in the September area depends significantly on anomalies in the seasonal ice area.

We find that ice age in the late 1980s and early 1990s declined markedly in agreement with *Rigor and Wallace* [2004] for the same reason they cite, owing to anomalously high flushing of older ice out through Fram Strait during high-index years of the Arctic Oscillation. However, when the AO returned to more neutral conditions, the ice age began to recover. In contrast, the perennial ice area, thickness and volume declined throughout the past two decades, with an apparent acceleration in the last decade, particularly in perennial ice volume. Younger ice classes began to decline again in the last few years of our integrations.

Although our model exhibits the expected relationship between ice age and thickness on multi-year and Northern Hemisphere-wide averages, we find that the correlation between ice age and thickness breaks down at the local scale (100s of kilometers and smaller) in individual years. Furthermore, on interannual time scales, the Northern Hemisphere average ice age is not well correlated with ice thickness, volume, or area. In fact, the September ice age is negatively correlated with September ice area, as anomalously low first-year coverage causes the average age in September to increase coincident with below average area. Thus our results show that ice age is not a good proxy for sea ice thickness in a given year, and it is no surprise that the area and thickness of sea ice may decline, while at the same time the ice age may have little trend.

Comparison of model output with remote sensing data is problematic partly because of disparities in scale, but also because of different methods for defining physical quantities, such as melt season length and ice age. Due to constant incorporation of young ice within the pack, the mean age of the simulated pack (or of ice in a grid cell) is younger than would be indicated by marking certain floes and aging them with each step of an advection algorithm or series of satellite images. The actual age of a given column of ice may be younger yet because of bottom accretion. Our ice age results are in good agreement with *Rigor and Wallace* [2004] in the later years of their integration, but their ice tends to be much older at the beginning of their analysis period. Thus their results show a substantial reduction in ice age, while ours do not.

Nevertheless, our model simulation reinforces the observationalists' story: older ice types have declined in the Arctic ice cover, partly through Fram Strait export. Some young ice survives to repopulate the older classes, but the area covered by ice less than 5 years old has shrunk considerably since 2000. In the coming decades, it is possible that the age of the Arctic ice pack will fluctuate between younger and older ice types, sometimes exhibiting bimodal age distributions as in the early 1990s, before becoming completely dominated by seasonal ice.

Acknowledgments. E. Hunke is supported by the Climate Change Prediction Program of the Department of Energy's Office of Biological and Environmental Research. C. Bitz gratefully acknowledges the support of the National Science Foundation through grant OPP0454843.

References

Arzel, O., T. Fichefet, and H. Goosse (2006), Sea ice evolution over the 20th and 21st centuries as simulated by the current AOGCMs, *Ocn. Mod.*, *12*, 401–415.

Belchansky, G. I., D. C. Douglas, and N. G. Platonov (2004), Duration of the Arctic sea ice melt season: Regional and interannual variability 1979–2001, *J. Clim.*, *17*, 67–80.

Belchansky, G. I., D. C. Douglas, and N. G. Platonov (2005), Spatial and temporal variations in the age structure of Arctic sea ice, *Geophys. Res. Lett.*, *32*, L18,504, doi:10.1029/2005GL023,976.

Bitz, C. M., and W. H. Lipscomb (1999), An energy-conserving thermodynamic sea ice model for climate study, *J. Geophys. Res.–Oceans*, *104*, 15,669–15,677.

Bitz, C. M., M. M. Holland, A. J. Weaver, and M. Eby (2001), Simulating the ice-thickness distribution in a coupled climate model, *J. Geophys. Res.–Oceans*, *106*, 2441–2463.

Bitz, C. M., M. M. Holland, E. C. Hunke, and R. E. Moritz (2005), Maintenance of the sea-ice edge, *J. Clim.*, *18*, 2903–2921.

Collins, W. D., C. M. Bitz, M. L. Blackmon, G. B. Bonan, C. S. Bretherton, J. A. Carton, P. Chang, S. C. Doney, J. J. Hack, T. B. Henderson, J. T. Kiehl, W. G. Large, D. S. McKenna, B. D. Santer, and R. D. Smith (2006), The Community Climate System Model Version 3 (CCSM3), *J. Clim.*, *19*, 2122–2143.

Comiso, J. C. (2002), A rapidly declining perennial sea ice cover in the Arctic, *Geophys. Res. Lett.*, *29*, doi:10.1029/2002GL015650.

Comiso, J. C. (2006), Abrupt decline in the Arctic winter sea ice cover, *Geophys. Res. Lett.*, *33*, L18,504, doi:10.1029/2006GL027,341.

Comiso, J. C., J. Yang, S. Honjo, and R. A. Krishfield (2003), Detection of change in the Arctic using satellite and in situ data, *J. Geophys. Res.*, *108*, 3384, doi:10.1029/2002JC001347.

Comiso, J. C., C. L. Parkinson, R. Gersten, and L. Stock (2008), Accelerated decline in the Arctic sea ice cover, *Geophys. Res. Lett.*, *35*, L01,703, doi:10.1029/2007GL031,972.

Connolley, W. M., J. M. Gregory, E. C. Hunke, and A. J. McLaren (2004), On the consistent scaling of terms in the sea ice dynamics equation, *J. Phys. Oceanogr.*, *34*, 1776–1780.

Flato, G. M., and W. D. Hibler (1995), Ridging and strength in modeling the thickness distribution of Arctic sea ice, *J. Geophys. Res.–Oceans*, *100*, 18,611–18,626.

Fowler, C., W. J. Emery, and J. Maslanik (2004), Satellite-derived evolution of Arctic sea ice age: October 1978 to March 2003, *IEEE Geosci. Rem. Sens. Lett.*, *1*, 71–74.

Gillett, N. P., M. Allen, R. E. McDonald, C. A. Senior, D. T. Shindell, and G. A. Schmidt (2002), How linear is the Arctic Oscillation response to greenhouse gases?, *J. Geophys. Res.*, *107*, ACL 1–1–1–7, 0.1029/2001JD000,589.

Gloersen, P., W. J. Campbell, D. J. Cavalieri, J. C. Comiso, C. L. Parkinson, and H. J. Zwally (1992), Arctic and Antarctic sea ice, 1978–1987: Satellite passive-microwave observations and analysis, *Tech. Rep. SP-511*, NASA.

Hibler, W. D. (1980), Modeling a variable thickness sea ice cover, *Mon. Wea. Rev.*, *108*, 1943–1973.

Holland, M. M., and C. M. Bitz (2003), Polar amplification of climate change in coupled models, *Climate Dyn.*, *21*, 221–232.

Hunke, E., and M. Holland (2007), Global atmospheric forcing data for Arctic ice-ocean modeling, *J. Geophys. Res.*, *112*, C06S14, doi:10.1029/2006JC003,640.

Hunke, E. C., and J. K. Dukowicz (2002), The Elastic-Viscous-Plastic sea ice dynamics model in general orthogonal curvilinear coordinates on a sphere—Effect of metric terms, *Mon. Wea. Rev.*, *130*, 1848–1865.

Hunke, E. C., and W. H. Lipscomb (2008), CICE: the Los Alamos Sea Ice Model, Documentation and Software User's Manual, version 4.0, *Tech. Rep. LA-CC-06-012*, Los Alamos National Laboratory, Los Alamos, New Mexico.

Johannessen, O. M., E. V. Shalina, and M. W. Miles (1999), Satellite evidence for an Arctic sea-ice cover in transformation, *Science*, *286*, 1937–1939.

Kiehl, J. T., and P. R. Gent (2004), The Community Climate System Model, Version Two, *J. Climate*, *17*, 3666–3682.

Kwok, R., and D. A. Rothrock (1999), Variability of Fram Strait ice flux and North Atlantic Oscillation, *J. Geophys. Res.*, *104*, 5177–5189.

Kwok, R., G. F. Cunningham, and S. S. Pang (2004a), Fram Strait sea ice outflow, *J. Geophys. Res.*, *109*, C01,009, doi:10.1029/2003JC001,785.

Kwok, R., H. J. Zwally, and D. Yi (2004b), ICEsat observations of Arctic Ocean sea ice: A first look, *Geophys. Res. Lett.*, *31*, L16,401, doi:10.1029/2004GL020,309.

Large, W., and S. Yeager (2004), Diurnal to decadal global forcing for ocean and sea-ice models: The data sets and flux climatologies, *NCAR Tech. Note NCAR/TN-460+STR*, CGD Division of the National Center for Atmospheric Research.

Large, W., and S. Yeager (2008), The global climatology of an interannually varying air-sea flux data set, *Clim. Dyn.*, Submitted.

Laxon, S., N. Peacock, and D. Smith (2003), High interannual variability of sea ice thickness in the Arctic region, *Nature*, *425*, 947–950.

Lipscomb, W. H. (2001), Remapping the thickness distribution in sea ice models, *J. Geophys. Res.–Oceans*, *106*, 13,989–14,000.

Lipscomb, W. H., and E. C. Hunke (2004), Modeling sea ice transport using incremental remapping, *Mon. Wea. Rev.*, *132*, 1341–1354.

Lipscomb, W. H., E. C. Hunke, W. Maslowski, and J. Jakacki (2007), Improving ridging schemes for high-resolution sea ice models, *J. Geophys. Res.–Oceans*, *112*, C03S91, doi:10.1029/2005JC003,355.

Lizotte, M. P. (2001), The contributions of sea ice algae to Antarctic marine primary production, *Amer. Zoologist*, *41*, 57–73.

Maslanik, J. A., C. Fowler, J. Stroeve, S. Drobot, J. Zwally, D. Yi, and W. Emery (2007), A younger, thinner Arctic ice cover: Increased potential for rapid, extensive sea-ice loss, *Geophys. Res. Lett.*, *34*, L24,501, doi:10.1029/2007GL032,043.

Nghiem, S. V., I. G. Rigor, D. K. Perovich, P. Clemente-Colon, J. W. Weatherly, and G. Neumann (2007), Rapid reduction of Arctic perennial ice, *Geophys. Res. Lett.*, *34*, L19,504, doi:10.1029/2007GL031,138.

Perovich, D. K. (2003), Complex yet translucent: the optical properties of sea ice, *Phys. B*, *338*, 107–114.

Perovich, D. K., J. A. Richter-Menge, K. F. Jones, and B. Light (2008), Sunlight, water, and ice: Extreme Arctic sea ice melt during the summer of 2007, *Geophys. Res. Lett.*, *35*, L11,501, doi:10.1029/2008GL034,007.

Rigor, I. G., and J. M. Wallace (2004), Variations in the age of Arctic sea-ice and summer sea-ice extent, *Geophys. Res. Lett.*, *31*, l09401, doi:10.1029/2004GL019492.

Rigor, I. G., J. M. Wallace, and R. L. Colony (2002), Response of sea ice to the Arctic Oscillation, *J. Climate*, *15*, 2648–2663.

Röske, F. (2001), An atlas of surface fluxes based on the ECMWF reanalysis–A climatological dataset to force global ocean general circulation models, *Tech. Rep. 323*, Max-Planck-Institut für Meteorologie.

Rothrock, D. A. (1975), The energetics of the plastic deformation of pack ice by ridging, *J. Geophys. Res.*, *80*, 4514–4519.

Rothrock, D. A., Y. Yu, and G. A. Maykut (1999), Thinning of the Arctic sea-ice cover, *Geophys. Res. Lett.*, *26*, 3469–3472.

Smith, D. M. (1998), Recent increase in the length of the melt season of perennial Arctic sea ice, *Geophys. Res. Lett.*, *25*, 655–658.

Thorndike, A. S., D. A. Rothrock, G. A. Maykut, and R. Colony (1975), The thickness distribution of sea ice, *J. Geophys. Res.*, *80*, 4501–4513.

Untersteiner, N. (1961), On the mass and heat budget of arctic sea ice, *Arch. Meteorol. Geophys. Bioklimatol., A*, *12*, 151–182.

Wadhams, P. (1990), Evidence for thinning of the Arctic ice cover north of Greenland, *Nature*, *345*, 795–797.

Wadhams, P., and N. R. Davis (2000), Further evidence of ice thinning in the Arctic Ocean, *Geophys. Res. Lett.*, *27*, 3973–3975.

WMO (1989), *Sea-Ice Nomenclature, No. 259 Suppl. No. 5*, World Meteorological Organization, Geneva, Switzerland.

Zhang, X., and J. E. Walsh (2006), Toward a seasonally ice-covered Arctic Ocean: Scenarios from the IPCC AR4 model simulations, *J. Clim.*, *19*, 1730–1747.

Figure Captions

Figure 1. (a) Volume and area of all Arctic ice, (b) volume, area and average thickness of perennial ice, (c) area of seasonal ice, (d) September seasonal ice area and total ice area anomaly from the 1977–2006 mean, and (e) area-weighted average age of perennial ice and the whole Arctic ice pack. The legend for panels (a)–(c) is in panel (b).

Figure 2. Winter (Nov.–Apr.) area flux through Fram Strait. Satellite-based observational data [*Kwok et al.*, 2004a] is dashed.

Figure 3. Monthly climatologies of perennial ice volume, area, thickness and area-weighted average age for the three decades shown in the lower panel.

Figure 4. Average March thickness of ice plotted against ice age, for three decades, and the *Maslanik et al.* [2007] proxy ice thickness estimates for 2003–2006. Model data are plotted only for age bins that are populated for all 10 years of each averaging period.

Figure 5. March ice thickness, in m, for (a) 1976, (b) 1986 (c) 1996, (d) 2006, overlain with ice age contours in black (2-year increments). The 15% area concentration contour is white.

Figure 6. (a) For September of each year, the total area of ice of age N indicated on the x-axis. For March of each year, (b) the total area of ice of age greater or equal to N, (c) the age of ice passing through Fram Strait (years). A 4-year running mean has been applied in (a) to smooth the seasonal cycle.

Figure 7. Area-weighted average age of perennial ice and the whole Arctic ice pack (a) in the control run, in which accretion at the bottom of the ice did not influence ice age, and (b) in the sensitivity run, in which bottom growth was included in the ice age.

	March		September	
	mean	trend	mean	trend
seasonal area	8.0	0.29	0.3	-0.01
perennial area	7.0	-0.42	5.5	-0.61
total ice area	15.0	-0.13	5.8	-0.62
average age	2.9	-0.27	6.5	-0.13

Table 1. Mean March and September 1977–2006 seasonal, perennial and total ice area (10^6 km^2), area-weighted average age (years), and their trends per decade, for the Northern Hemisphere.

	Smith [1998]		*Belchansky et al.* [2004]		CICE	
	mean	trend	mean	trend	mean	trend
melt onset	164	-0.7	169	-4.0	141	-4.9
freeze onset	240	+3.7	238	+1.4	233	+1.8
melt season	75	+4.5	68	+5.5	91	+6.7

Table 2. Mean 1979–1996 melt and freeze onset dates (Julian day) and melt season length (days) for perennial ice, and their trends (days per decade).

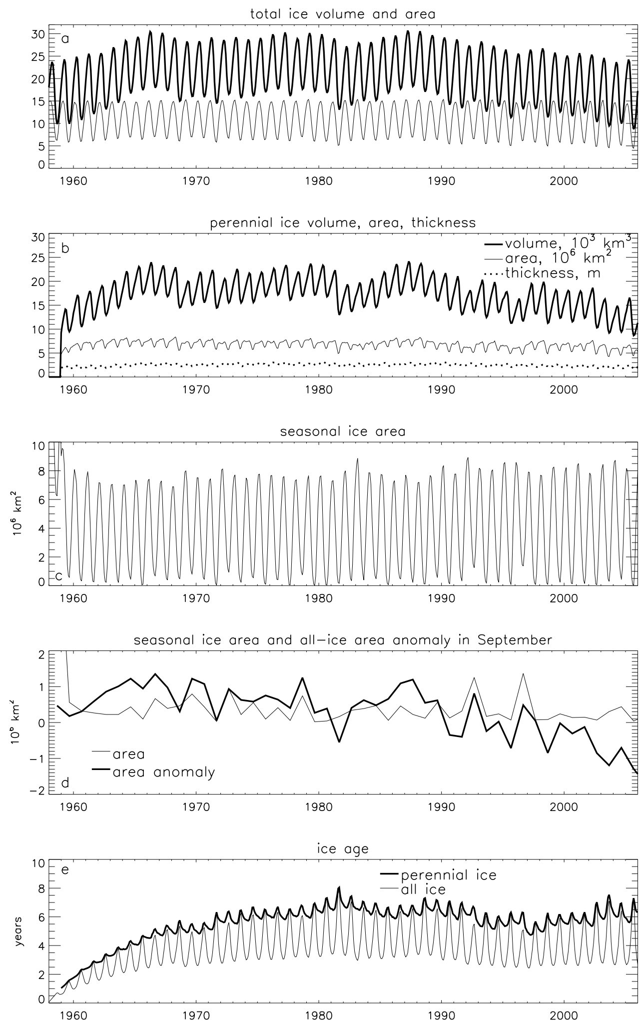

Figure 1. (a) Volume and area of all Arctic ice, (b) volume, area and average thickness of perennial ice, (c) area of seasonal ice, (d) September seasonal ice area and total ice area anomaly from the 1977–2006 mean, and (e) area-weighted average age of perennial ice and the whole Arctic ice pack. The legend for panels (a)–(c) is in panel (b).

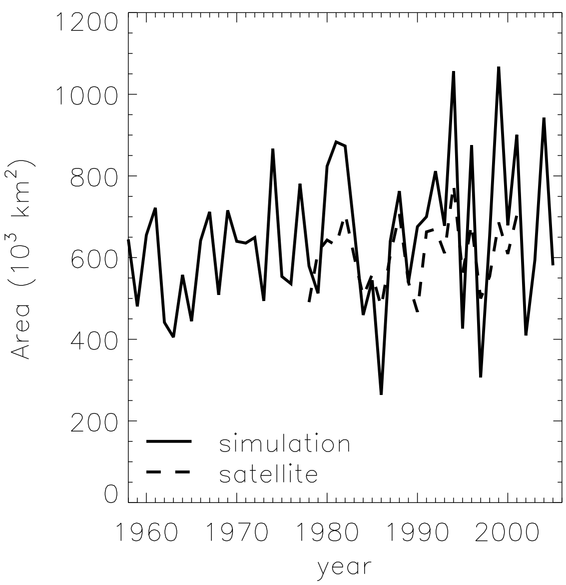

Figure 2. Winter (Nov.–Apr.) area flux through Fram Strait. Satellite-based observational data [*Kwok et al.*, 2004a] is dashed.

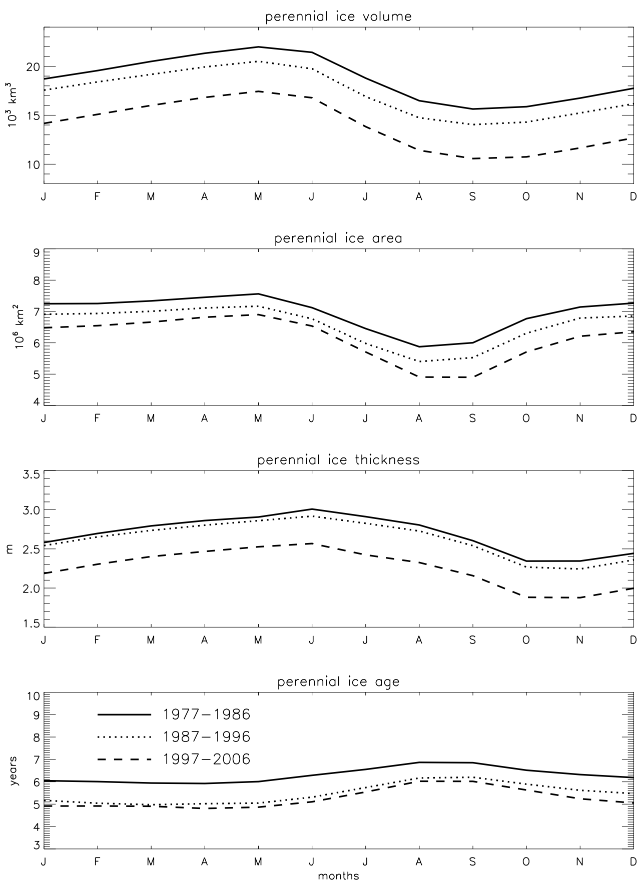

Figure 3. Monthly climatologies of perennial ice volume, area, thickness and area-weighted average age for the three decades shown in the lower panel.

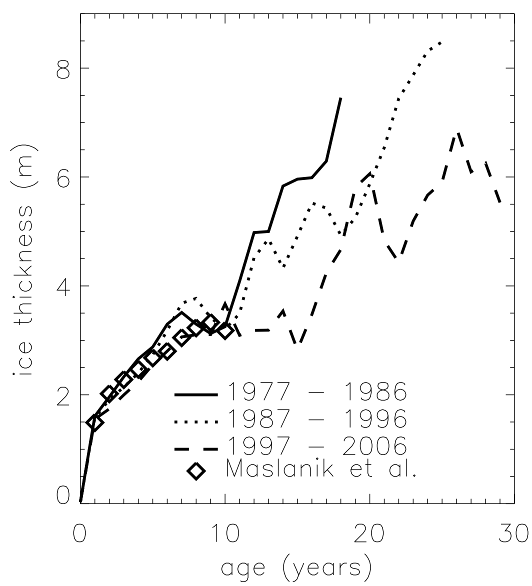

Figure 4. Average March thickness of ice plotted against ice age, for three decades, and the *Maslanik et al.* [2007] proxy ice thickness estimates for 2003–2006. Model data are plotted only for age bins that are populated for all 10 years of each averaging period.

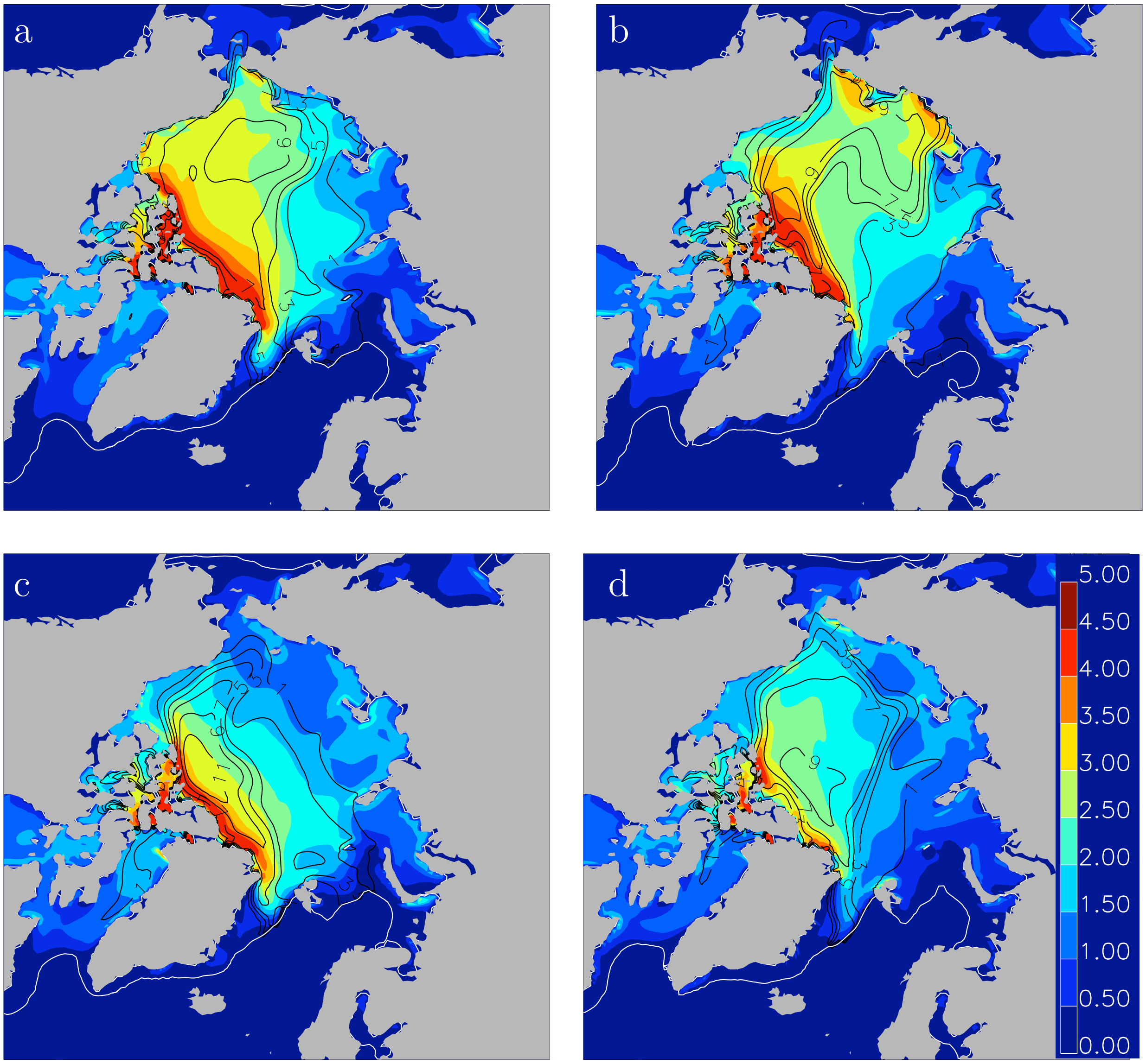

Figure 5. March ice thickness, in m, for (a) 1976, (b) 1986 (c) 1996, (d) 2006, overlain with ice age contours in black (2-year increments). The 15% area concentration contour is white.

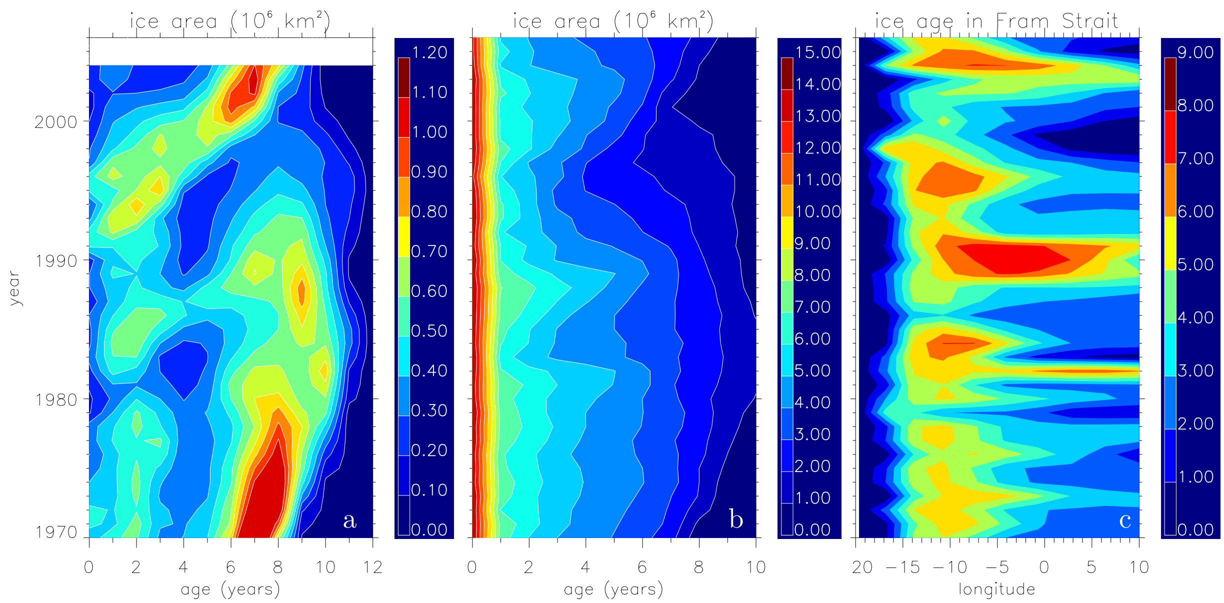

Figure 6. (a) For September of each year, the total area of ice of age N indicated on the x-axis. For March of each year, (b) the total area of ice of age greater or equal to N, (c) the age of ice passing through Fram Strait (years). A 4-year running mean has been applied in (a) to smooth the seasonal cycle.

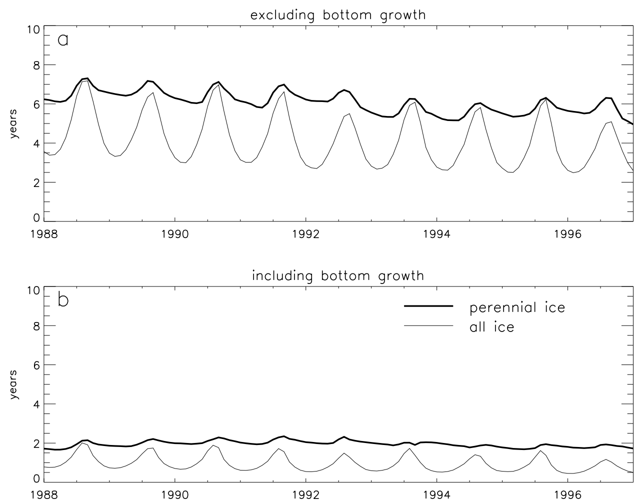

Figure 7. Area-weighted average age of perennial ice and the whole Arctic ice pack (a) in the control run, in which accretion at the bottom of the ice did not influence ice age, and (b) in the sensitivity run, in which bottom growth was included in the ice age.